Surface & Coatings Technology xxx (2012) xxx–xxx

Contents lists available at SciVerse ScienceDirect

Surface & Coatings Technology

journal homepage: www.elsevier.com/locate/surfcoat

Electrical and optical characteristics of cylindrical non-thermal atmospheric-pressure dielectric barrier discharge plasma sources

Yui Lun Wu, Jungmi Hong, Zihao Ouyang, Tae S. Cho *, D.N. Ruzic

Center for Plasma Material Interactions, Department of Nuclear Plasma and Radiological Engineering, University of Illinois at Urbana-Champaign, Urbana, IL 61801, USA

ARTICLE INFO

Available online xxxx

Keywords:
Plasma jet
Dielectric barrier discharge
Co-axial ring electrodes
Propagation speed
Ionization front
VQ Lissajous

ABSTRACT

Two types of cylindrical non-thermal dielectric barrier discharge plasma sources working at atmospheric pressure have been investigated and the electrical and optical characteristics were determined. The configurations compared are ring-and-rod and double-ring. At 30 kHz frequency and 62 W fixed input power, the electrical characteristics: V–I and V–Q Lissajous curves were measured. The capacitances, energies dissipated, and powers consumed for plasma generation have been quantified. Light emission characteristics of the two configurations were also measured at the main discharge region between the electrodes as well as at the afterglow plasma region. The propagation speed of ionization front of afterglow plasma has been estimated to be 0.5–1.3 cm/μs in this experiment.

1. Introduction

Non-thermal atmospheric pressure plasma has numerous applications in many areas of industry, such as purification of gas or liquid state pollutants, cleaning of volatile organic compounds, modification of surface properties, and more recently, biomedical applications. It is favored in these applications since it is simple in structure, environmentally safe and has excellent performance [1–4]. Non-thermal plasmas operating at atmospheric pressure without a massive and expensive vacuum chamber system allow expanding scope of potential applications. In recent years, many researchers have been intensively studying the application to biomedical area such as blood coagulation, tissue sterilization, ablation of cancer cells, and eradication of pathogens. These atmospheric plasma sources are generally produced by dielectric barrier discharge (DBD), which has the benefit of avoiding the glow-to-arc transition. Several DBD configurations for atmospheric plasma sources have been studied with several kilovolts in voltage and several tens of kilohertz in frequency [3,4]. Capacitive coupled coaxial electrode systems are used widely and they consist of a rod electrode at the center of the cylindrical dielectric tube, and another ring electrode wrapped around the tube. To date, atmospheric DBD plasmas find most applications in surface modification. Atmospheric plasma treatment has already proven its ability to promote the adhesion between layers and the surface properties have been changed to hydrophilic or hydrophobic depending on process conditions [5]. Furthermore, powder and fine particle treatments by atmospheric DBD plasma have also been attempted to change the surface properties [6]. Unlike planar surface treatment, fine particles or powders are introduced into the tube along with process gas and the powder gets treated by passing through the atmospheric plasma region, thus the gas conductance of the tube becomes important when it comes to treating significant amount of powders in a mass production system. The electrode inside the tube can significantly reduce the conductance and can be contaminated by the powder. To address this issue, other types of cylindrical capacitive coupled coaxial electrode system with no electrode inside the dielectric tube have been used [7,8].

In this paper, we have compared the electrical and optical characteristics of two typical cylindrical capacitive coupled coaxial electrode configurations, as shown in Fig. 1. The surface treatment results using those two structures are also discussed.

2. Experimental results and discussions

We have considered two types of cylindrical atmospheric pressure plasma source in order to investigate the influence of the electrode configuration on electrical and optical characteristics. The first one is called ring-and-rod structure, which has a rod shaped electrode inside of tube and a ring shaped electrode outside of tube, as shown in Fig. 1(a). Another one is called double-ring structure, having two ring shaped electrodes wrapped outside of the tube, as shown in Fig. 1(b). We used 200 mm long quartz tube as the dielectric barrier, of which outer diameter and thickness were 15 mm and 1 mm, respectively. The rod and ring electrodes were made of stainless steel tube (6.35 mm outer and 3 mm inner diameters) and copper tape (20 mm width), respectively. The two electrodes were separated by 25 mm. The working gas used in this study was helium with flow rate of 30 lpm (liter per minute). 30 kHz sinusoidal AC voltage was applied to one electrode while another was kept ground. As shown in Fig. 1(c), the voltage and current were measured with a 1000:1 voltage probe (P6015A, Tektronix) and a current

* Corresponding author. Tel.: +1 217 333 1750; fax: +1 217 244 0179.
E-mail address: tscho@illinois.edu (T.S. Cho).

0257-8972/$ – see front matter © 2012 Elsevier B.V. All rights reserved.
http://dx.doi.org/10.1016/j.surfcoat.2012.09.043

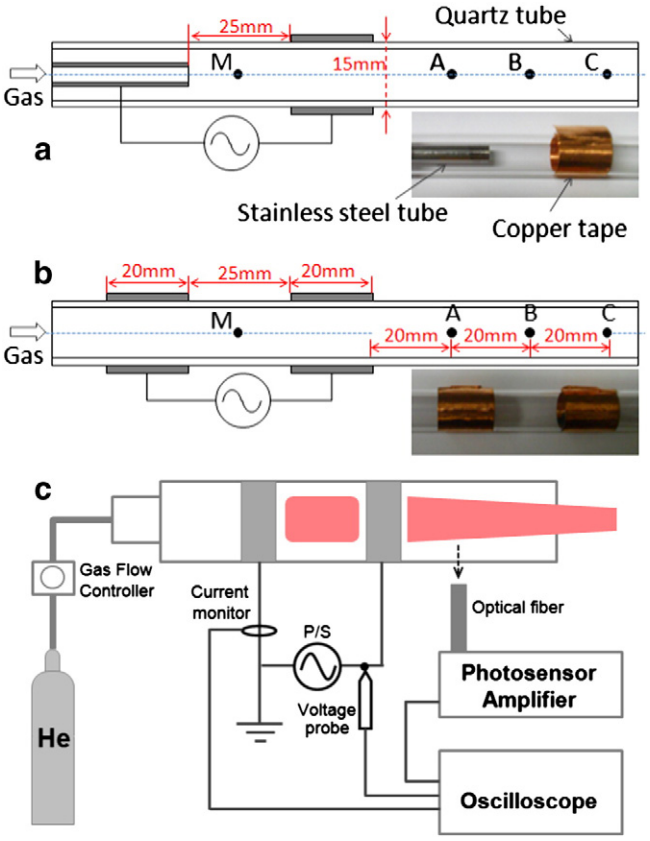

Fig. 1. Schematics of dielectric barrier discharge plasma sources in two different configurations: ring-and-rod (a) and double-ring structures (b) and experimental setup (c).

monitor (4100, Pearson Electronics), respectively. The light emission from the plasma was monitored with an optical fiber and a photosensor amplifier (C6386, Hamamatsu) which has a broad spectral range of 400 nm–1100 nm.

Fig. 2 shows the main discharge plasma generated between two electrodes and the afterglow plasma propagating toward the tube exit at the same input power of 62 W. The ring-and-rod structure shows similar main discharges and afterglow plasmas, independent of the high voltage and ground electrode configuration, as shown in Fig. 2(a). On the other hand, the formation of afterglow plasma from the double-ring structure depends on which electrodes are grounded or powered. When the high voltage is applied to the electrode closer to the gas inlet side, no afterglow plasma could be observed. When the high voltage is applied to the electrode further from the gas inlet an afterglow plasma propagates all the way past the exit. As for this experiment, high voltage was consistently applied to the copper electrode closer to the tube exit for both structures.

The significant difference between ring-and-rod and double-ring structures is the number of electrode covered with dielectrics which affects plasma discharge phenomena, such as breakdown voltage and current. Fig. 3 shows the current–voltage characteristic curves for both configurations. The currents increase linearly with the increasing voltages for both cases but the current of ring-and-rod structure increases more rapidly than in the case of double-ring structure. The filamentary discharge starts to occur beyond voltages of 6.5 kV and 8.5 kV for ring-and-rod and double-ring, respectively. In the case of 4.6 kV for ring-and-rod and 6.7 kV for double-ring, both powered at 62 W, same lengths of afterglow plasmas were observed, as shown in Fig. 2. At the same power operation, the double-ring derives less current at higher voltage because both electrodes were covered with dielectric layer while one of the electrodes in ring-and-rod was exposed directly to the plasma. Two times thicker dielectric layer between electrodes were used, and higher discharge voltage and lower discharge current were observed. It is observed that the ring-and-rod structure is a lower voltage and higher current device than the double-ring structure.

Fig. 4 shows the voltage and current waveforms and the light emissions, which were measured at the position M in Fig. 1, at the center of the main discharge region between electrodes. The breakdown voltage can be estimated from the light emission signal. The discharge ignites at the voltage of ± 2.8 kV with peak current of 30 mA for ring-and-rod structure, while double-ring structure starts to generate plasma at ± 4.3 kV with 19 mA current. The light intensity from ring-and-rod structure is two times stronger than that from double-ring structure at the same power operation, as ring-and-rod structure has a higher current which corresponds to a stronger discharge. Using one period of voltage and current waveforms in Fig. 4, the V–Q Lissajous characteristic curves could be plotted as shown in Fig. 5. The slopes of the V–Q Lissajous curve before breakdown, a-a′ and b-b′, represent capacitances of the ring-and-rod and double-ring structures which are estimated to be 11.3 ± 0.6 pF and 5.2 ± 0.3 pF, respectively. Considering an actual charging path of the structures as capacitive loads, the charging path of the ring-and-rod structure is shorter than that of the double-ring, which results in higher capacitance. The energies dissipated for discharge per one cycle, which can be calculated from the area under the closed pattern of V–Q Lissajous plot, are 1.27 ± 0.06 mJ for the ring-and-rod and 0.98 ± 0.05 mJ for the double-ring. The power consumptions

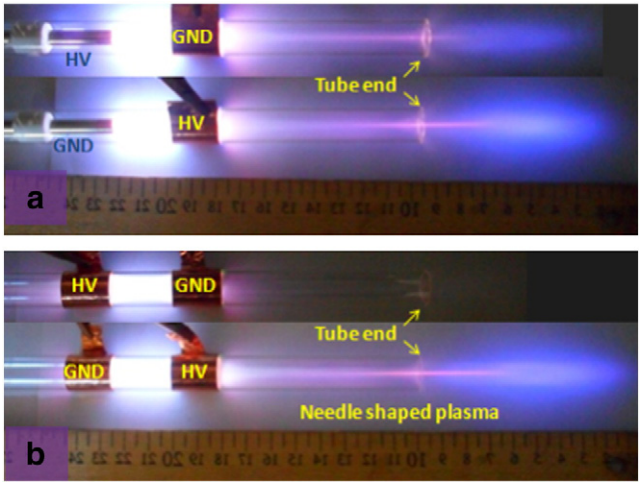

Fig. 2. Atmospheric pressure helium plasma from ring-and-rod (a) and double-ring structures (b).

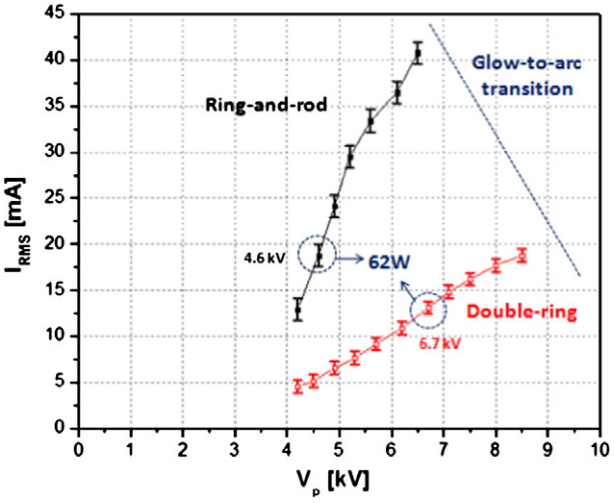

Fig. 3. V–I characteristic curves of ring-and-rod and double-ring structures.

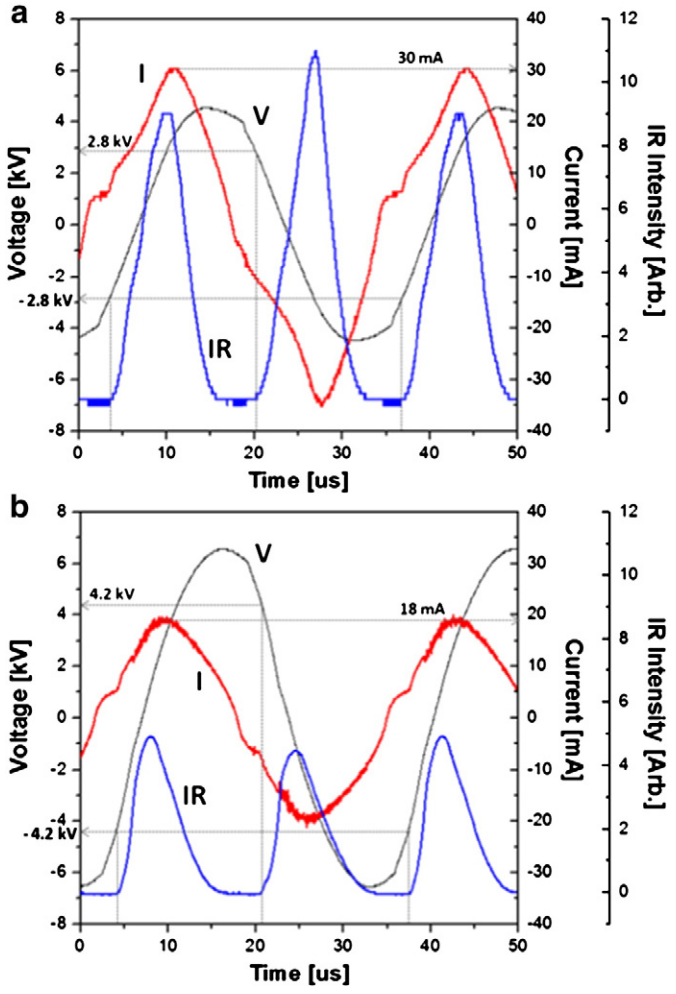

Fig. 4. Voltage and current waveforms at input power of 62 W and light emission profiles from ring-and-rod (a) and double-ring structures (b).

for the discharge can be calculated from the energies dissipated at 30 kHz driving frequency. They were found to be 38.1 W for the ring-and-rod and 29.4 W for the double-ring. Note that the ring-and-rod structure consumed 61% of the input power for plasma generation and 39% for charging and discharging the capacitive load, while the double-ring only spent 47% of input power for plasma generation.

Fig. 6 shows the light emission intensity measured at three points in afterglow plasma region at point A, B and C in Fig. 1, which are 20 mm, 40 mm, and 60 mm away from the electrode end, respectively. The propagation speeds of ionization front of afterglow plasma between the regions A–B and B–C are 0.7 cm/μs and 1.2 cm/μs for the ring-and-rod, and 0.5 cm/μs and 1.3 cm/μs for the double-ring, which is almost 5–10 times faster than thermal velocity of helium at ambient temperature of ~0.1 cm/μs. Based on the results, it is obvious that the propagation speed of the ionization front is getting faster when it approaches the tube exit, where a thin long needle-shaped plasma was observed. The afterglow plasma close to the electrode end looks more diffusive while the plasma near the tube exit looks more focused. These characteristics might be caused by the nozzle's effect on the charge distribution in the gas around the tube exit which causes the ionization front to move faster. The gas speed of 3.8 m/s, which can be calculated from the gas flow rate (30 lpm) and inner diameter of tube (13 mm), is much slower than the speed of ionization front of 5 km/s–13 km/s. Based on the estimation of the electron drift velocity at the work done by X. Lu and M. Laroussi [9], the electron drift velocity in our system can also be calculated to be 23 km/s, which has similar order of magnitude as our afterglow plasma. The propagation speed of our system seems to be slower than previous reports because of the differences in size of the plasma torch, driving waveforms, and gas conditions [9–11]. It is also interesting to note that no propagation into regions A, B and C is observed when the double-ring electrode closer to the exit is grounded because no electric field exists along the tube length propelling the ionization front.

The light emissions from the ring-and-rod structure are more intense than that from double-ring structure at every position measured, even though the main discharge of the ring-and-rod seems stronger than that of the double-ring. The peak of the light emission from the ring-and-rod showed up ~15 μs after the trigger (t = 0 μs) which is much slower than the double ring. The reason for this is the attribution from the charged particles to propagate and then ionize the neutral gas molecules. Based on light emissions from the main discharge region, the ring-and-rod structure generates more charged particles than the double-ring structure, but significant amount of

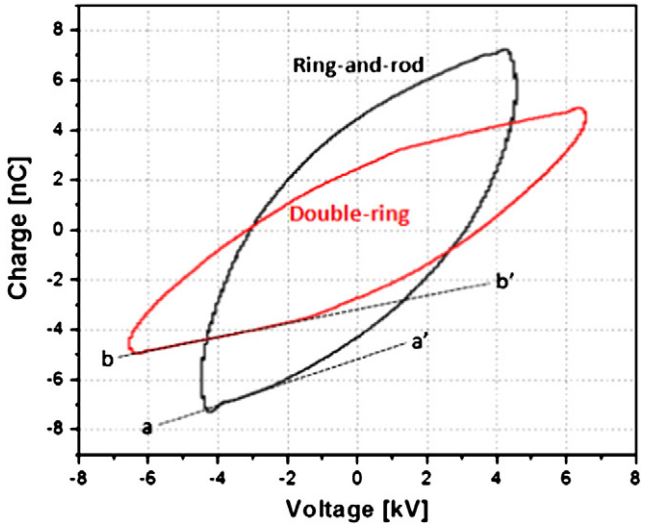

Fig. 5. V–Q Lissajous characteristic curves.

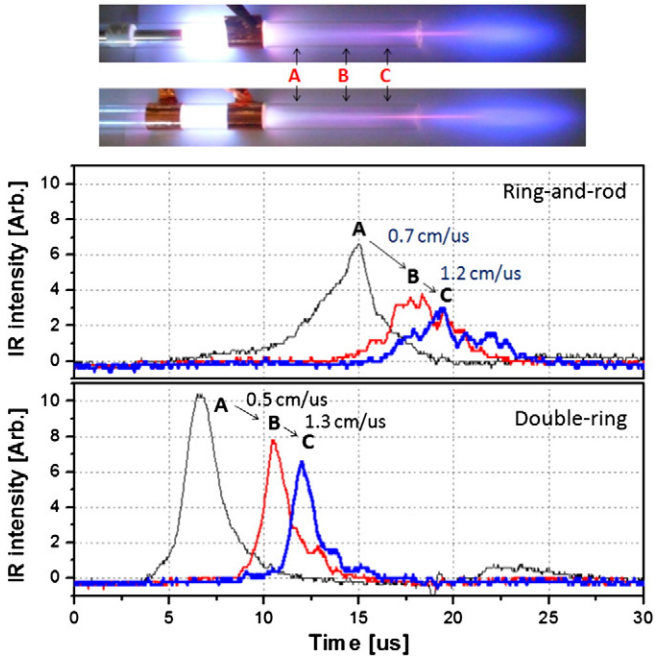

Fig. 6. Light emission profiles measured at 2 cm, 4 cm and 6 cm away from the main discharge region.

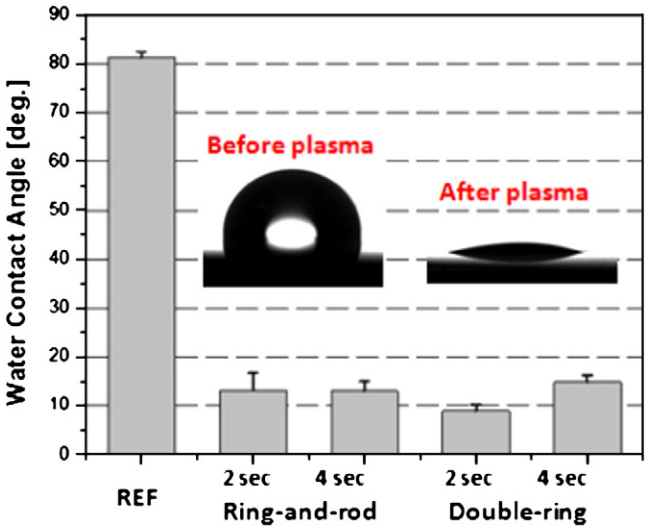

Fig. 7. Water contact angle measurement for untreated and treated polyimide film with afterglow plasma from ring-and-rod and double-ring structures.

charged particles could be attracted back into the bare metal electrode and only about half of the charged particles including wall charges could move to the propagation region and contribute to breakdown. On the other hand, most of the charged particles including wall charges produced in double-ring could be used to ionize the neutrals in propagation region for the double-ring structure.

To compare performance, a polyimide film has been treated with both plasma sources driven at same power (62 W). The polyimide film was positioned 30 mm away from the tube exit and treated with helium plasmas for a 2 s and 4 s exposure time. The water contact angle of the polyimide film decreases significantly from ~80° to 10–15° for both devices, as shown in Fig. 7. A non-thermal atmospheric He plasma made the hydrophobic polyimide surface very hydrophilic.

3. Conclusions

Tests were performed on two types of cylindrical non-thermal dielectric barrier discharge plasma sources working at atmospheric pressure. The electrical and optical characteristics of the atmospheric pressure plasmas were studied. From the V–I characteristics, the ring-and-rod type plasma source works as a low-voltage and high-current device, while the double-ring displays a high-voltage and low-current character. The ring-and-rod structure generates stronger main discharge, which can be confirmed by the power consumption for plasma generation. However its afterglow plasma is weaker than that of the double-ring structure, which means there are critical losses of charged particle to the bare metal electrode. On the other hand, the double-ring structure has stronger afterglow plasma than the ring-and-rod even though it has weaker main discharge, because there is no significant loss of charged particle to the electrodes as they are perfectly covered with dielectrics. Although light intensities from afterglow plasmas are quite different, the surface treatment results for polyimide film are very similar. This result could be clarified in further studies. Lastly, propagation speeds of ionization front of afterglow plasmas from both structures were measured to be 0.5–1.3 cm/μs in this experiment.

References

[1] U. Kogelschatz, Plasma Chem. Plasma Process. 23 (1) (2003) 1.
[2] J.Y. Kim, J. Ballato, P. Foy, T. Hawkins, Y. Wei, J. Li, S. Kim, Small 6 (14) (Jul. 2010) 1474.
[3] G. Cho, H. Lim, J.H. Kim, D.J. Jin, G.C. Kwon, E.H. Choi, H.S. Uhm, IEEE Trans. Plasma Sci. 39 (5) (2011) 1234.
[4] H.W. Lee, S.H. Nam, A.-A.H. Mohamed, G.C. Kim, J.K. Lee, Plasma Process. Polym. 7 (3–4) (Mar. 2010) 274.
[5] E. Stoffels, A.J. Flikweert, W.W. Stoffels, G.M.W. Kroesen, Plasma Sources Sci. Technol. 11 (4) (Nov. 2002) 383.
[6] M. Kogoma, S. Hashimoto, K. Tanaka, J. Photopolym. Sci. Technol. 19 (2) (2006) 231.
[7] S. Ogawa, A. Takeda, M. Oguchi, K. Tanaka, T. Inomata, M. Kogoma, Thin Solid Films 386 (2) (May 2001) 213.
[8] Y. Sawada, M. Kogoma, Powder Technol. 90 (3) (Mar. 1997) 245.
[9] X. Lu, M. Laroussi, J. Appl. Phys. 100 (2006) 063302.
[10] M. Laroussi, T. Akan, Plasma Process. Polym. 4 (2007) 777.
[11] J.S. Oh, J.L. Walsh, J.W. Bradley, Plasma Sources Sci. Technol. 21 (2012) 034020.

Please cite this article as: Y.L. Wu, et al., Surf. Coat. Technol. (2012), http://dx.doi.org/10.1016/j.surfcoat.2012.09.043